

# FROM ASTRID TO BRAHMA - THE ROLE OF OVERMASSIVE BLACK HOLES IN LITTLE RED DOTS IN COSMOLOGICAL SIMULATIONS

PATRICK LACHANCE<sup>1,\*</sup>, AKLANT KUMAR BHOWMICK<sup>2,3,4</sup>, RUPERT A.C. CROFT<sup>1</sup>, TIZIANA DI MATTEO<sup>1</sup>, YIHAO ZHOU<sup>1</sup>,  
 FABIO PACUCCI<sup>5,6</sup>, LAURA BLECHA<sup>7</sup>, PAUL TORREY<sup>2,3,4</sup>, YUEYING NI<sup>8</sup>, NIANYI CHEN<sup>9</sup>, AND SIMEON BIRD<sup>10</sup>

<sup>1</sup> McWilliams Center for Cosmology and Astrophysics, Department of Physics, Carnegie Mellon University, Pittsburgh, PA 15213 USA

<sup>2</sup> University of Virginia 530 McCormick Rd Charlottesville, VA 22904, USA

<sup>3</sup> Virginia Institute for Theoretical Astronomy, University of Virginia, Charlottesville, VA 22904, USA

<sup>4</sup> The NSF-Simons AI Institute for Cosmic Origins, USA

<sup>5</sup> Center for Astrophysics | Harvard & Smithsonian, 60 Garden St, Cambridge, MA 02138, USA

<sup>6</sup> Black Hole Initiative, Harvard University, 20 Garden St, Cambridge, MA 02138, USA

<sup>7</sup> Department of Physics, University of Florida, Gainesville, FL 32611, USA

<sup>8</sup> Michigan Institute for Data and AI in Society, 500 Church Street, Suite 600, Ann Arbor, MI 48109

<sup>9</sup> Institute for Advanced Study, 1 Einstein Dr, Princeton, NJ 08540  
 and

<sup>10</sup> Department of Physics & Astronomy, University of California, Riverside, 900 University Ave., Riverside, CA 92521, USA

*Version December 19, 2025*

## ABSTRACT

We leverage the overmassive black holes ( $M_{\text{BH}}/M_* \approx 0.1$ ) present in a realization of the BRAHMA cosmological hydrodynamic simulation suite to investigate their role in the emission of the unique “little red dot” (LRD) objects identified by the James Webb Space Telescope (JWST). We find that these black holes can produce LRD-like observables when their emission is modeled with a dense gas cloud shrouding the active galactic nucleus (AGN). Between redshifts 5 and 8, we find the number density of LRDs in this simulation to be  $2.04 \pm 0.32 \times 10^{-4} \text{Mpc}^{-3}$ , which is broadly consistent with current estimates for the total LRD population from JWST. Their emission in the rest-frame visible spectrum is dominated by their AGN, which induces the red color indicative of LRDs via a very strong Balmer break. Additionally, the elevated mass of the black holes reduces the temperature of their accretion discs. This shifts the peak of the AGN emission towards longer wavelengths, and increases their brightness in the rest-frame visible spectrum relative to lower mass black holes accreting at the same rate. These simulated LRDs have very minimal dust attenuation ( $A_V = 0.21 \pm 0.12$ ), limiting the amount of dust re-emission that would occur in the infrared, making them very likely to fall below the observed detection limits from observatories like the Atacama Large Millimeter Array (ALMA). In contrast to the BRAHMA box, the ASTRID simulation produces systematically smaller black holes and predicts LRD number densities that are more than two orders of magnitude lower than current measurements. We therefore conclude that the presence of black holes that are overmassive relative to their host galaxy, and enshrouded in dense gas, is necessary for AGN-dominated LRD models to reproduce both the observed properties and abundances of JWST LRD populations.

*Subject headings:* Surveys, Hydrodynamical simulations, High-redshift Universe, Galaxy evolution, Active galaxies

## 1. INTRODUCTION

Early JWST observations revealed a population of objects dubbed “little red dots” (LRDs; Matthee et al. 2023; Labb   et al. 2023; Kocevski et al. 2023; Harikane et al. 2023; Furtak et al. 2023). These objects are compact in appearance, and feature a very red color in the rest-frame optical bands, and a flat or blue color in the rest-frame

UV bands. Since their discovery, it has been unclear what they are, with initial proposals including compact star-forming galaxies and dust-attenuated AGN (Baggen et al. 2023; Barro et al. 2023; Labb   et al. 2023; Maiolino et al. 2024; Guia et al. 2024).

A variety of follow-up observations have been conducted on these objects, including JWST spectroscopy (Kokorev et al. 2024), X-ray (Ananna et al. 2024; Yue et al. 2024b; Maiolino et al. 2025), and infrared observa-

\*E-mail: plachance@cmu.edu

tions (Casey et al. 2025), which have identified a number of common features of the spectra of LRDs. They are X-ray weak (Akins et al. 2025; Ananna et al. 2024; Yue et al. 2024b; Maiolino et al. 2025; Pacucci & Narayan 2024), feature broad Balmer emission lines (Wang et al. 2024; Ma et al. 2024), and a significant Balmer break (Setton et al. 2024; Labbe et al. 2024), and there are upper limits on their infrared (Casey et al. 2025) and radio (Perger et al. 2025) emission. This combination of features, along with their UV and visible colors and compact morphology, has made them difficult to reconcile with existing models of galaxy formation, stellar populations, and AGN emission. Dust-attenuated sources, both stellar and AGN, would likely be far brighter in the IR than observed LRDs due to dust reprocessing (Casey et al. 2024). Traditional AGN emission models without significant dust attenuation would not produce the visible red colors of observed LRDs, and may produce more X-ray emission than is expected from current observations (Shen et al. 2020). Dense stellar sources would generally lack the broad emission lines seen in LRD spectra, but may be able to produce them in specific circumstances (Pérez-González et al. 2024; Hvizing et al. 2025; Baggen et al. 2024; Guia et al. 2024; Pacucci et al. 2025).

Recent results have placed an increasing amount of importance on the Balmer break as a characteristic feature of the LRD spectrum (Liu et al. 2025), and a variety of works have proposed AGN-centric models which feature spectral energy densities (SEDs) that differ significantly from those that are based on catalogs of low redshift quasars (Shen et al. 2020). Two approaches have been taken to this. One derives an adjustment to the bolometric corrections for AGN using a purely empirical approach based on the observations of two of the brightest observed LRDs, and extrapolate a possible AGN SED from the observed emission, and detection limits (Greene et al. 2025). The other utilizes photoionization modeling to produce AGN spectra, and attempt to determine the AGN parameters that fit observed LRD spectra. This process has been applied to CAPERS-LRD-z9 (Taylor et al. 2025) MoM-BH\*-1 (Naidu et al. 2025), and *The Cliff* (de Graaff et al. 2025), and all three cases find atypical properties for the AGN and surrounding gas.

Specifically, they find that enshrouding the AGN within a very dense cloud of gas, which produces a pronounced Balmer break, results in spectra that can reproduce many of the observed properties of LRDs. The Balmer break creates the red color in the rest optical region, and the bright AGN produces the broad emission lines in that wavelength region. The dense gas environment would also limit the amount of X-ray emission that could escape the AGN, which aligns with the observations that find the vast majority of LRDs are X-ray weak. Additionally, the reddening provided by the gaseous environment limits the amount of dust attenuation that is required to appear as an LRD, which also limits the dust re-emission in the infrared, aligning with the observed upper limits on LRD infrared emission. Further motivation for these models is provided in Inayoshi & Maiolino (2025), which performs an in depth analysis of the spectral features of “gas-enshrouded” AGN, and in Jeon et al. (2025) which posits direct collapse black holes (DCBHs) as progenitors of the AGN in LRDs, and finds modeling their emission with the dense gas SED reproduces the

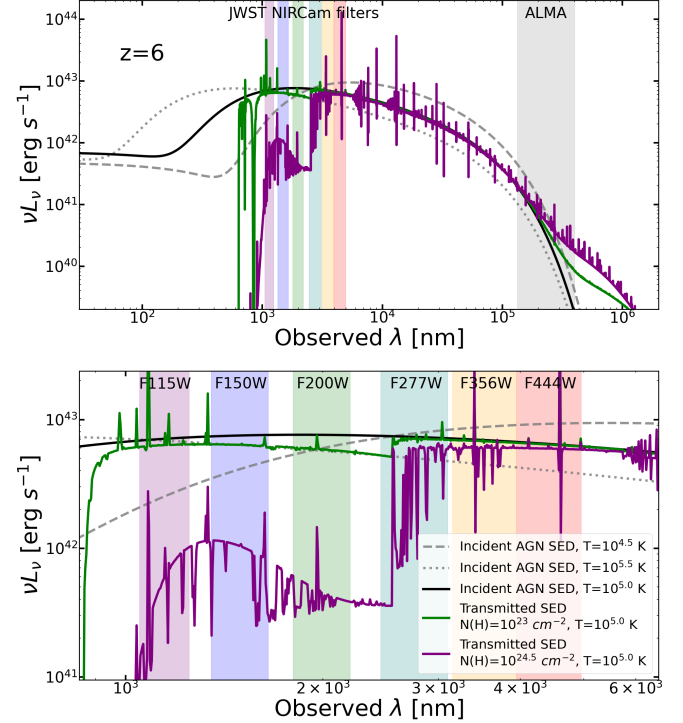


FIG. 1.— Example of the AGN Spectra used as input for, and output by, `CLOUDY`. We are placing this example object at  $z = 6$  to provide relevant comparisons with observational bands. The top panel shows a broad view of the spectrum, spanning the infrared and X-ray regions. The lower panel zooms in on the JWST NIRCam wavelength range. The black line is the incident AGN spectrum in `CLOUDY`, which is processed through the surrounding gas cloud. We have chosen a temperature of  $T = 10^{5.0}$  K for the example AGN. The green, and purple lines show different transmitted spectra based on the properties of the gas cloud. The green line is the cloud properties used in LaChance et al. (2025), and the purple spectrum is produced by the “gas-enshrouded” model we use in this work. The dashed and dotted grey lines are the incident AGN spectra produced by AGN with temperatures  $T = 10^{4.5}$  K, and  $T = 10^{5.5}$  K respectively.

spectra of observed LRDs.

Cosmological simulations may provide unique insights into these objects, as they couple large scale gravity+hydrodynamics with a wide range of relevant astrophysical processes such as cooling, star formation, black hole seeding, accretion, and feedback, to produce statistically large populations of galaxies and BHs. Given the breadth of possibilities for the nature of LRDs and the remaining uncertainties about their core physical properties, such as black hole and stellar mass, identifying and analyzing LRDs in simulations could provide clarity on the properties and environments necessary for their production.

Despite their advantages, cosmological simulations do not perform all of the astrophysical processes that are necessary for the modeling of LRDs. This includes many aspects crucial to modeling observations such as the production of emission from AGN and stars, and the attenuation of that emission by dust. As such, post-processing is required to produce observables from the simulation output. For the AGN this is primarily done via radiative transfer modeling with software like `CLOUDY` (Gunasekera et al. 2025), which is coupled to properties of the black holes from the simulation and produces the spectra of those black holes. As the radiative transfer occurs on

length scales that are well below the resolution of the cosmological simulation, there are aspects of the model, such as the properties of the gas cloud surrounding the AGN, which cannot be inferred from the simulation. Similarly, the stellar emission is based on the properties of the star particles present in the simulation, via a coupling to a stellar synthesis model, as each star particle in the simulation represents many individual stars.

We have performed an initial analysis of the LRD population in the **ASTRID** simulation (Ni et al. 2022; Bird et al. 2022; Ni et al. 2025; Zhou et al. 2025) in a previous work (LaChance et al. 2025), and identified a very limited number of LRDs, which represent only a small fraction of the observed number density. We performed this analysis before the “gas-enshrouded” AGN model was prevalent, which limited the amount of LRDs that were found due to smaller Balmer break in the AGN SED. Additionally, the black hole population in **ASTRID** at high redshifts aligns more closely to the pre-JWST predictions, so there are no black holes with the high  $M_{\text{BH}}/M_{\ast}$  ratios inferred from recent JWST observations.

The study of LRDs is closely intertwined with investigations of the population of potentially “overmassive” black holes observed at similarly early epochs, some of which have been identified as LRDs (Pacucci et al. 2023; Durodola et al. 2025; Taylor et al. 2024; Furtak et al. 2024; Jones et al. 2025). While there is the possibility that the masses of these objects have been overestimated (Greene et al. 2025; Brooks et al. 2024, 2025), it remains unclear which interpretation is correct. Further exploration of the physical conditions capable of producing such overmassive black holes—and whether these conditions also give rise to LRD populations consistent with observations—may help resolve this ambiguity.

The recent **BRAHMA** simulations (Bhowmick et al. 2024b,c) have systematically explored a wide range of black-hole seed model variations to identify the conditions necessary for producing overmassive black holes at high redshift. In particular, Bhowmick et al. (2024c) demonstrated that overmassive black holes at  $z \sim 4-7$  can be assembled if heavy  $\sim 10^5 M_{\odot}$  seeds form in sufficiently abundant numbers and subsequently grow efficiently through black-hole mergers occurring within  $\lesssim 750$  Myr following their host-galaxy mergers. These conditions may be optimistic, given the stringent requirements for direct-collapse black-hole formation and the possibility of longer delay times for black-hole mergers (Ma et al. 2021; Partmann et al. 2024). Nevertheless, the **BRAHMA** simulations provide an ideal arena for isolating and understanding the influence of black-hole “overmassiveness” on the occurrence of LRDs in cosmological simulations. Accordingly, in this work we focus on the **BRAHMA** simulation volume that produces the most overmassive black holes—consistent with current JWST constraints—by adopting a deliberately lenient model for heavy  $\sim 10^5 M_{\odot}$  seed formation, and we search for LRD-like objects in mock observations of the resulting galaxy and AGN populations at  $z \sim 4-8$ .

This paper is organized as follows: A description of the simulations used in this work, and the methods for creating mock observations are presented in section 2. We detail the properties of the both the “little red dots”, and the general population of galaxies within **BRAHMA** and investigate which properties are critical to the production

of an LRD in section 3. We finish the paper with a summary and discussion of our work, along with highlighting future projects that could further our understanding of “little red dots”.

## 2. METHODS

### 2.1. The **BRAHMA** Simulation Suite

The **BRAHMA** cosmological simulation suite (Bhowmick et al. 2024b,c) was run with the **AREPO** cosmological magnetohydrodynamics (MHD) code (Springel 2010; Pakmor et al. 2011, 2016; Weinberger et al. 2020), which solves gravity using a PM–Tree algorithm (Barnes & Hut 1986) and evolves the gas using the ideal MHD equations on a dynamically moving Voronoi mesh. The simulations adopt the Planck Collaboration et al. (2016) cosmology and are initialized at  $z = 127$  using **MUSIC** (Hahn & Abel 2011). Many components of the galaxy formation model follow the **IllustrisTNG** framework (Springel et al. 2018; Pillepich et al. 2018; Nelson et al. 2018; Naiman et al. 2018; Marinacci et al. 2018; Nelson et al. 2019), including radiative cooling from primordial and metal species, star formation in gas above the density threshold of  $0.13 \text{ cm}^{-3}$ , stellar evolution and chemical enrichment, and stellar feedback implemented via hydrodynamically decoupled galactic winds. Black hole accretion follows an Eddington-limited Bondi prescription with a radiative efficiency of  $\epsilon_r = 0.2$ , while AGN feedback is modeled using the two-mode thermal/kinetic scheme employed in **IllustrisTNG**.

A key feature of the **BRAHMA** simulations is their use of physically motivated BH seeding prescriptions (Bhowmick et al. 2021, 2022, 2024a) that are designed based on popular seed formation channels—Pop III remnants, nuclear star clusters (NSCs), and direct-collapse black holes (DCBHs). The suite includes a large number of cosmological volumes that systematically explore a broad range of seed-model variants, spanning seed masses of  $\sim 10^3-10^5 M_{\odot}$  and incorporating diverse gas-based seeding criteria that depend on density, metallicity, Lyman–Werner radiation intensity, angular momentum, and environmental richness. This led to the largest simulation-based systematic exploration of how different seed-model variations imprint distinct predictions on a variety of high- $z$  BH observables. Bhowmick et al. (2024c) demonstrated that variations in seed modeling exert a strong influence on the high- $z$  stellar-mass–BH-mass relation. An overmassive relation at  $z \sim 4-7$ —as suggested by JWST observations Pacucci et al. (2023); Juodžbalis et al. (2025)—requires models that produce a substantial population of massive ( $\sim 10^5 M_{\odot}$ ) seeds that subsequently merge efficiently, i.e., within  $\lesssim 750$  Myr of their host galaxy mergers. They also showed that even though BH mergers had the dominant contribution to the BH mass assembly, the simulated AGN luminosity functions were broadly consistent with high- $z$  JWST observations.

In this work, we analyze the BH populations from one of the **BRAHMA** volumes employing our most lenient heavy-seed prescription. In this model, seeds of mass  $M_{\text{seed}} = 1.5 \times 10^5 M_{\odot}$  ( $10^5 M_{\odot}/h$ ) are planted in halos that host a sufficient reservoir of *dense* ( $n_{\text{H}} > 0.13 \text{ cm}^{-3}$ ) and *metal-poor* ( $Z < 10^{-4} Z_{\odot}$ ) gas. The dense, metal-poor gas mass threshold is set to five times

the seed mass. BHs are repositioned toward the local gravitational potential minimum over a region defined by the 1000 nearest gas neighbors, and mergers are triggered when multiple BHs reside within this region. [Bhowmick et al. \(2024c\)](#) applied this seeding model to an  $[18 \text{ Mpc}]^3$  box (with  $512^3$  DM particles) and demonstrated that the resulting BH populations are systematically overmassive at  $z \sim 4-7$ , in broad agreement with many of the overmassive BHs inferred from *JWST*. Here, we apply the same prescription to a larger  $[36 \text{ Mpc}]^3$  box (with  $1024^3$  DM particles) to investigate whether—and under what physical conditions—these overmassive BH populations could manifest observationally as the LRDs recently discovered by *JWST*.

## 2.2. The ASTRID Simulation

In addition to the BRAHMA simulation, we use the ASTRID simulation ([Ni et al. 2022; Bird et al. 2022; Ni et al. 2025; Zhou et al. 2025](#)) as a point of comparison throughout this work, as we have comparable analysis from this simulation, and it was run with a standard set of cosmological parameters (based on the Planck Survey [Planck Collaboration et al. \(2020\)](#)) and astrophysical models. It is run with the Smoothed Particle Hydrodynamics (SPH) code MP-GADGET ([Feng et al. 2018](#)). The simulation volume is  $[369 \text{ Mpc}]^3$ , with an initial particle load of  $2 \times 5500^3$  particles. The resulting mass resolution is  $\sim 6.5$  times lower than the BRAHMA box we use, and similar to the Illustris TNG100 and EAGLE simulations, with a simulation volume larger than Illustris TNG300 ([Illustris TNG: Springel et al. 2018; Nelson et al. 2018; Marinacci et al. 2018; Naiman et al. 2018; EAGLE: Schaye et al. 2015](#)).

The star formation is performed with the model described in [Feng et al. \(2016\)](#), which is based on the model originally developed in [Springel & Hernquist \(2003\)](#). There is an additional correction to handle the formation of molecular hydrogen, and corresponding adjustments to the star formation model in low metallicity environments per [Krumholz & Gnedin \(2011\)](#). The gas cooling follows the prescription of [Katz et al. \(1996\)](#), with an implementation of dense gas self-shielding per [Rahmati et al. \(2013\)](#). The full description of the stellar and gas processes are detailed in [Bird et al. \(2022\)](#) and [Ni et al. \(2022\)](#).

Similar to BRAHMA, ASTRID employs a modified Bondi–Hoyle accretion prescription, but with an additional boost factor of 100 and a lower radiative efficiency of 0.1. In addition, ASTRID permits mildly super-Eddington accretion, up to twice the Eddington limit. The AGN feedback model in ASTRID is broadly similar to that in BRAHMA, with both thermal and kinetic feedback modes present. Despite a relatively lenient accretion model compared to BRAHMA, black hole growth in ASTRID—particularly within low-mass galaxies—is significantly slower than in BRAHMA. The primary driver of this difference is the black hole seeding procedure. In ASTRID, halos are seeded with initial black holes of mass  $\sim 4.4 \times 10^4-4.4 \times 10^5 M_\odot$  only once both the total halo mass and stellar mass exceed thresholds of  $\geq 7.4 \times 10^9 M_\odot$  and  $3 \times 10^6 M_\odot$ , respectively. This criterion is substantially more restrictive than that adopted in the BRAHMA volume used here, where black hole seeds can

form in halos with masses as low as  $\sim 10^8 M_\odot$ . Furthermore, ASTRID incorporates a subgrid dynamical friction model to capture black hole dynamics ([Chen et al. 2022](#)), whereas the particular BRAHMA box analyzed in this work employs black hole repositioning. Together, these differences lead to more efficient merger-driven growth in low-mass galaxies in BRAHMA, a behavior that is largely absent in ASTRID. While the repositioning scheme is likely to overestimate merger-driven growth in BRAHMA, the substantially higher seeding frequency alone implies that BRAHMA should generically experience a larger number of black hole mergers than ASTRID, even when coupled to with subgrid dynamical friction model. We will explore these effects in greater detail in forthcoming work (Zhao et al., in prep.; Bhowmick et al., in prep.). As emphasized earlier, the primary focus of this work is to investigate the implications of such an overmassive black hole population in BRAHMA for the formation and properties of LRDs.

## 2.3. Mock Observation Pipeline

We use a nearly identical mock-observation process described in [LaChance et al. \(2025\)](#) to calculate photometric magnitudes for each source. The one adjustment we make is to the AGN SED model, which is described in section 2.3.1. We begin by calculating the intrinsic stellar emission of each star particle with the Binary Population and Spectral Population Synthesis model (BPASS version 2.2.1; [Stanway & Eldridge 2018](#)). These spectra are subject to dust attenuation via the interstellar medium (ISM), which we calculate using a simple power law dust model:

$$\tau_{\text{ISM}}(\lambda) = -\kappa_{\text{ISM}} \Sigma(x, y, z) \left( \frac{\lambda}{0.55\mu\text{m}} \right)^\gamma \quad (1)$$

where  $\tau_{\text{ISM}}(\lambda)$  is the optical depth,  $\kappa_{\text{ISM}}$  is an attenuation strength tuning parameter that we assign a value of  $10^{4.1}$  ([Bird et al. 2022](#)),  $\Sigma(x, y, z)$  is the metal surface density for each star, and  $\gamma$  is the slope of the dust model. We set  $\gamma = -1.0$ , which falls between the slopes of the Small Magellanic Cloud model ([Pei 1992](#)) and the ‘starburst’ model ([Calzetti et al. 2000](#)). For further details, see [Wilkins et al. \(2017\); LaChance et al. \(2024\)](#).

Young stars (Age  $\leq 10$  Myr) are also subject to stellar birth cloud attenuation and can produce nebular emission. The nebular emission is produced following the procedure outlined in [Wilkins et al. \(2020\)](#), and the birth cloud attenuation follows the process detailed in [Vijayan et al. \(2021\)](#). We use [SynthObs](#) ([Wilkins et al. 2020](#)) to implement the entire stellar portion of the pipeline.

We calculate the observed magnitude in each band by summing the luminosities of all star particles and black holes within twice the stellar half-mass radius, thereby approximating the aperture used in observation while reducing compute time by skipping the full imaging process for each source. For the sources that meet the color criteria described in section 3.1, we create a mock observed image to calculate the compactness of the source. We do so following the process described in [LaChance et al. \(2024\)](#) for the creation of mock CEERS observations.

### 2.3.1. AGN SED production

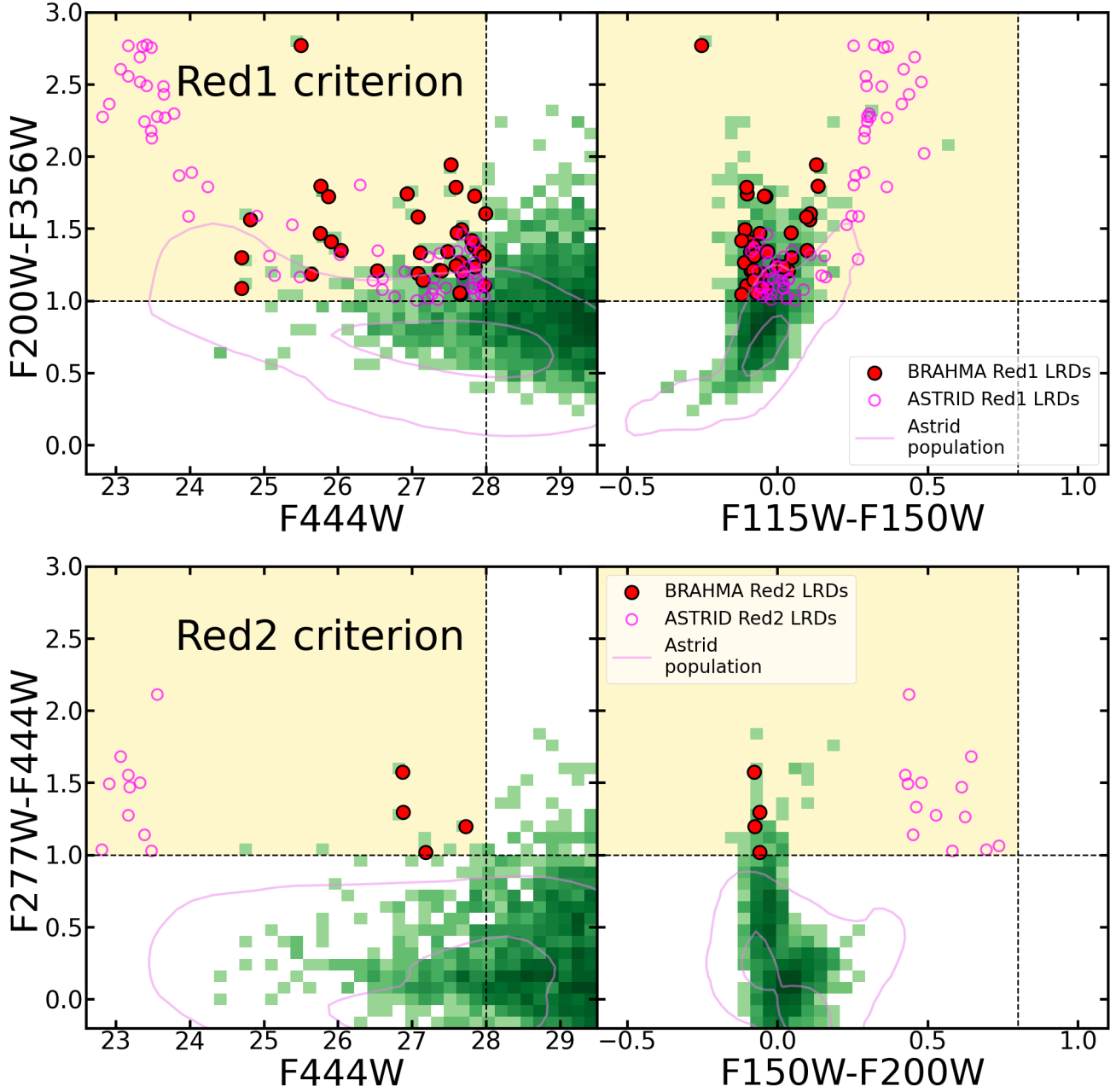


FIG. 2.— Color-Color and Color-Magnitude plots for the colors and magnitudes used in the “little red dot” criteria. The top panel shows sources F200W-F356W color vs. F444W magnitude, and F115W-F150W color. These are the primary factors in determining if a source meets the Red1 LRD criterion. The bottom panel shows sources F277W-F444W color vs. F444W magnitude, and F150W-F200W color. These are used in the Red2 LRD criterion. In order for a source to be considered a Red1 LRD it must be above the horizontal dashed line, and to the left of the vertical dashed line (falling within the highlighted regions) in both plots in the upper panel. The same is true for the Red2 criterion, and the plots in the bottom panel. The green 2D histogram shows the population of sources in BRAHMA. The magenta contours contain  $1\sigma$  and  $3\sigma$  of sources in the ASTRID simulation. The LRDs identified in BRAHMA are marked with red circles, and the LRDs found in ASTRID are shown with open magenta circles. Both panels include all of the sources in the snapshots we analyzed ( $z = 5 - 8$ ).

We use an altered version of the AGN SED model from LaChance et al. (2025), created with the `cloudy` (Gunnasekera et al. 2025) photoionization code. This model uses the same AGN input SED with default parameters of  $-1.4$  for  $\alpha_{\text{ox}}$ ,  $-0.5$  for  $\alpha_{\text{UV}}$ , and  $-1.0$  for  $\alpha_X$ , and is run with temperatures ranging from  $10^4$ K to  $10^6$ K, which are used to determine the AGN SED for a given black hole. The temperature of the AGN SED in `CLOUDY` corresponds to the peak of the bump in the incident SED, but the overall SED still represents the temperature profile

of an accretion disc. The temperature at a given radius in the accretion disc is given by

$$T_{\text{BH}}(r) = \left( \frac{3Gm_{\text{BH}}\dot{m}_{\text{BH}}}{8\pi\sigma r^3} \right)^{1/4} (1 - \sqrt{r_{\text{isco}}/r})^{1/4} \quad (2)$$

where  $T_{\text{BH}}(r)$  is the temperature at distance  $r$  from the black hole,  $\dot{m}_{\text{BH}}$  is the accretion rate of the black hole, and  $r_{\text{isco}}$  is the radius of the inner most circular orbit for the black hole ( $r_{\text{isco}} = \frac{6Gm_{\text{BH}}}{c^2}$ ). This equation

Simulation	“standard” AGN	“gas-enshrouded” AGN
BRAHMA	$9.9 \pm 7.0 \times 10^{-6}$	$2.04 \pm 0.32 \times 10^{-4}$
ASTRID	$8.4 \pm 2.0 \times 10^{-8}$	$3.68 \pm 0.43 \times 10^{-7}$

TABLE 1

THE NUMBER DENSITY OF “LITTLE RED DOTS” IN THE BRAHMA AND ASTRID SIMULATIONS WHEN APPLYING THE MORE AGN MODEL OF [LaChance et al. \(2025\)](#) (“STANDARD” AGN) AND THE “GAS-ENSHROUDED” AGN MODEL DESCRIBED IN SECTION 2.3.1. THE MODELS DIFFER IN THEIR VOLUME AND SURFACE DENSITY OF HYDROGEN, AND GAS TURBULENCE. THE “STANDARD” MODEL HAS A LESS DENSE, AND LESS DEEP GAS CLOUD SURROUNDING THE AGN THAN THE “GAS-ENSHROUDED” MODEL, AND ALSO LACKS THE TURBULENT MOTION PRESENT IN THE “GAS-ENSHROUDED” MODEL. ALL VALUES IN THE TABLE HAVE UNITS OF  $[\text{Mpc}^{-3}]$ , WITH POISSON UNCERTAINTIES.

is maximized at a radius of  $r = \frac{49}{36}r_{isco}$ , and we use the temperature at this radius to determine the input temperature for CLOUDY.

All SEDs are produced with a set bolometric luminosity of  $10^{43.5}\text{erg/s}$ , and are scaled to match the exact luminosity of each black hole in the simulation. We calculate the luminosity of each black hole with the equation

$$L_{\text{bol}} = \eta \dot{m}_{BHC} c^2 \quad (3)$$

where  $\eta$  is radiative efficiency, for which we use the assigned values of  $\eta = 0.2$  &  $0.1$  for BRAHMA and ASTRID respectively.

We use equation 1 to calculate the dust attenuation of the AGN due to the interstellar medium (ISM), but use a value of  $\gamma = -2.0$  rather than  $-1.0$ . Dust attenuation plays a very minimal role in the emission of AGN in BRAHMA, as we shall show later, but we retain this AGN-specific adjustment to remain consistent with [LaChance et al. \(2025\)](#). The metal surface density for each black hole is calculated along the line-of-sight, using the SPH kernels of the gas particles in its host galaxy, following the procedure of [Ni et al. \(2022\)](#).

We make the following changes to the gas properties of the AGN SED model we used in [LaChance et al. \(2025\)](#) in order to produce the “gas-enshrouded” AGN SED we use throughout this work. We change the hydrogen column density from  $\log(N(\text{H})/\text{cm}^{-2}) = 23.0$  to  $24.5$  and the inner hydrogen density from  $\log(n(\text{H})/\text{cm}^{-3}) = 9.0$  to  $9.5$  along with introducing turbulence to the gas cloud with velocity  $v_{\text{turb}} = 400 \text{ km/s}$ , while keeping the inner radius of  $\log(r/\text{cm}) = 16.7$ . This iteration of the “gas-enshrouded” AGN model is motivated by the increasing importance of the Balmer break to the spectral profile of LRDs, and the similar “gas-enshrouded” AGN models used in [Inayoshi & Maiolino \(2025\)](#); [Naidu et al. \(2025\)](#); [Taylor et al. \(2025\)](#); [Jeon et al. \(2025\)](#). The exact values of these parameters varies between works, with  $n(\text{H}) = 10^8 - 10^{11} \text{ cm}^{-2}$ ,  $N(\text{H}) = 10^{23} - 10^{26} \text{ cm}^{-3}$  and  $v_{\text{turb}} = 300 - 500 \text{ km/s}$ . We chose values near the center of the middle of the range for each parameter, but future work could investigate this parameter space to determine the values that are most conducive to recreating the LRD population from observations.

The impact of these changes in the UV-visible range is shown in Figure 1 as the difference between the green and purple lines. The previous AGN SED model deviated minimally from the input SED (black line), featuring a very small Balmer Break, and the production of emission lines. The “gas-enshrouded” AGN has a much

more significant Balmer break, with wider absorption features due to the turbulence present in the gas. This large Balmer Break is sufficient to produce the red rest-frame optical color of an LRD as long as it is prominent compared to the AGN’s host galaxy.

In Figure 1 we also show multiple incident SEDs at fixed luminosity with different temperatures to demonstrate the impact of temperature on AGN emission (the grey and black lines). The lower temperature SED peaks at longer wavelengths than the higher temperature SED, making it brighter in the long wavelength JWST filters.

### 3. RESULTS

We apply the mock-observation pipeline described above to generate synthetic images and spectra for simulated AGN–galaxy populations in both the BRAHMA and ASTRID volumes. We then identify sources that satisfy the criteria for classification as “little red dots” (LRDs), and analyze both the full AGN population and the LRD subset to determine which physical properties cause an AGN–host galaxy system to appear as an LRD.

#### 3.1. Little Red Dot Identification

We use LRD criteria similar to those used by UNCOVER ([Greene et al. 2024](#); [Labbe et al. 2025](#)). We apply a magnitude cut on the F444W emission of  $m_{\text{F444W}} < 28.0$  to ensure the objects are cleanly detected. Sources are then selected based on their colors, which must fit at least one of the Red1 or Red2 criteria,

$$\text{Red1} = (\text{F115W}-\text{F150W} < 0.8) \text{ and}$$

$$(\text{F200W} - \text{F277W} > 0.7) \text{ and}$$

$$(\text{F200W} - \text{F356W} > 1.0),$$

$$\text{Red2} = (\text{F150W}-\text{F200W} < 0.8) \text{ and}$$

$$(\text{F277W} - \text{F356W} > 0.7) \text{ and}$$

$$(\text{F277W} - \text{F444W} > 1.0)$$

and their compactness in the F444W band, which must meet the following criterion:

$$\text{compact} = f_{\text{F444W}}(0.4'')/f_{\text{F444W}}(0.2'') \leq 1.7$$

where  $f_{\text{F444W}}(0.4'')$  is the flux detected in the F444W band inside an aperture with a diameter of  $0.4''$ . We include both the Red1 and Red2 criteria to reduce the risk of selection effects arising from the shifting of rest-frame emission across the observation bands. This is particularly important with regard to the observed wavelength of the Balmer break, as it produces a significant change in the colors of these objects as its location shifts across the F277W filter from redshift  $z = 5$  to  $8$  ( $\lambda_{\text{obs}} \sim 2.2 \mu\text{m}$  to  $\sim 3.3 \mu\text{m}$ ). Broadly, this results in sources at redshifts 5 and 6 being selected by the Red1 criterion, and sources at redshifts 7 and 8 being selected by the Red2 criterion. All sources are evaluated using both selection criteria; however, for presentation purposes, we highlight the Red1 selection and corresponding colors for sources at redshifts 5 and 6, and the Red2 selection for sources at redshifts 7 and 8. Additionally, we assign each source a “Rest-visible Color” value based on the criterion associated with its redshift. For sources at redshifts  $z = 5$

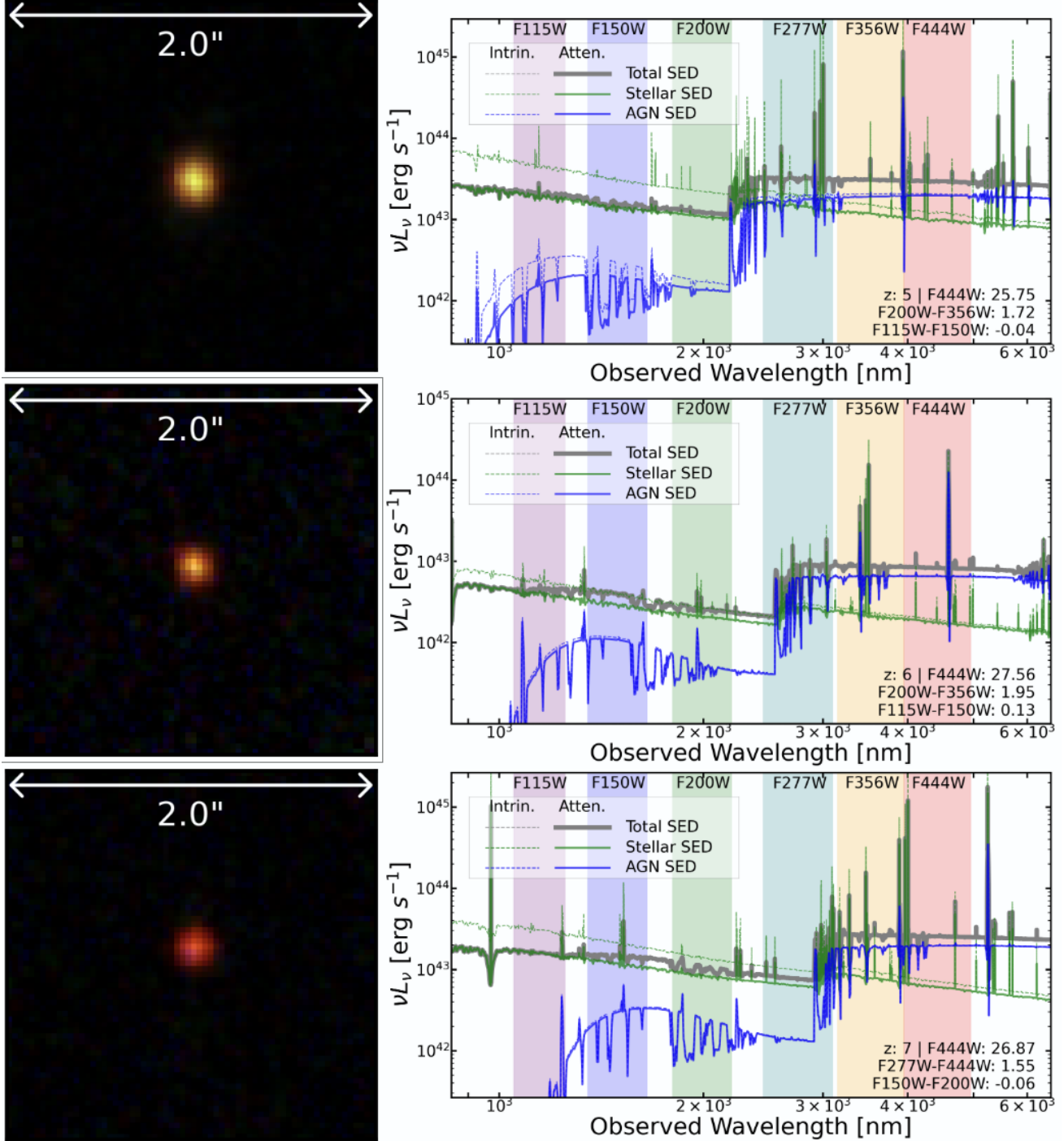


FIG. 3.— Mock JWST observations of three of the “Little Red Dots” found in the BRAHMA simulation. The images on the left are produced with the F444W, F277W, and F150W filters as the red, green, and blue channels, respectively. The spectra on the right show the total source spectrum in grey, the stellar component in green, and the AGN component in blue. The dashed lines indicate the spectra before dust attenuation is applied.

and 6, Rest-visible Color is defined as  $F200W - F356W$ , while for sources at redshifts  $z = 7$  and 8, Rest-visible Color is defined as  $F277W - F444W$ .

We present the color selection criteria in Figure 2. We find a total of 41 in these four snapshots of BRAHMA, with 37 of them fitting the Red1 color criterion, and 4 fitting the Red2 criterion. We find an additional 57 sources which meet the color criteria, but are too extended, and thus don’t meet the compactness criterion. In ASTRID we

find a total of 74 LRDs, all of which meet the Red1 color criterion, and 13 of which meet the Red2 criterion.

In addition to the BRAHMA results, we also show the  $1\sigma$  and  $3\sigma$  contours for the population of sources in ASTRID, and the LRDs identified within ASTRID. Notably, we do reprocess the sources in ASTRID with the “gas-enshrouded” AGN model described in section 2.3.1, and apply the LRD criteria outlined in section 3.1. We do this to ensure the two populations are as comparable as pos-

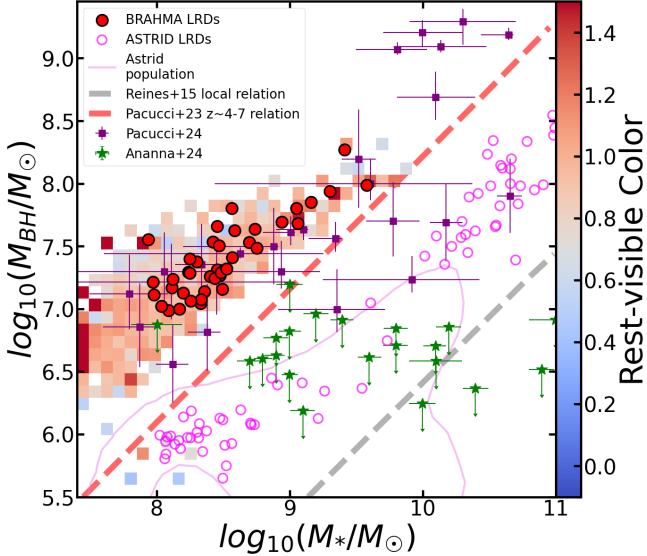


FIG. 4.— The  $M_{\text{BH}} - M_*$  for the black holes and their host galaxies in the BRAHMA and ASTRID simulations. The 2D histogram shows the overall BRAHMA population. It is colored by the mean “Rest-visible Color” in each cell, where “Rest-visible Color” is F200W-F356W for  $z=5,6$  sources, and F277W-F444W for  $z=7,8$  sources. The magenta contours contain  $1\sigma$  and  $3\sigma$  of sources in the ASTRID simulation. The LRDs identified in BRAHMA are marked with red circles, and the LRDs found in ASTRID are shown with open magenta circles. The purple square dataset is comprised of AGN fits from Maiolino et al. (2024); Harikane et al. (2023); Übler et al. (2023); Stone et al. (2024); Furtal et al. (2024); Yue et al. (2024a) compiled in Pacucci & Loeb (2024). The green star dataset was produced in Ananna et al. (2024) from the X-ray observations of some LRDs. We also include the local relation per Reines & Volonteri (2015) and an inferred  $z \sim 4 - 7$  relation from Pacucci et al. (2023)

sible, isolating just the impact of the black hole seeding model of the BRAHMA realization we analyze. To highlight this, we also produce mock observations of the BRAHMA simulation with the AGN emission model of LaChance et al. (2025), and present the number densities of all four configurations (BRAHMA vs ASTRID and standard vs “gas-enshrouded” AGN SED) in table 1. The observed number density of LRDs in this epoch is  $\sim 10^{-4} \text{Mpc}^{-3}$  (Pacucci & Loeb 2025; Kocevski et al. 2025), indicating the BRAHMA with “gas-enshrouded” AGN modeling is the only configuration that can reproduce an LRD population that is comparable with observations. Both ASTRID configurations, and BRAHMA with a standard AGN emission model all under-predict the LRD density by  $\sim 1 - 3$  orders of magnitude.

We present the mock observations of three of these LRDs at different redshifts in figure 3. Visually, all three appear as compact objects, dominated by a large source of emission at their centers. Their spectra reveal the importance of the Balmer break, as it produces the red color in the long wavelength JWST bands. All three LRDs feature AGN which dominate the emission above the Balmer break, but are outshone by their host galaxy below the break. This indicates that the host galaxy is primarily responsible for the rest-UV emission of LRDs. In all three sources there is minimal dust attenuation, especially in the rest-visible range. The stellar components show slightly more dust attenuation than the AGN due to the attenuation of young stars from the remnants of their birth cloud.

### 3.2. Black hole and galaxy properties

We analyze the black hole and galaxy properties of the LRDs in BRAHMA, and compare with both the overall population of galaxies in BRAHMA, and the LRD and overall population of ASTRID.

In Figure 4 we show the populations on the  $M_{\text{BH}} - M_*$  plane. For galaxies of a given stellar mass, we find that the BRAHMA population, including the LRDs, generally has black hole masses that are one to two orders of magnitude higher than in ASTRID, and overlaps with the observed high-mass black holes detected with JWST (Pacucci et al. 2023). Within the BRAHMA population, there is minimal correlation between black hole mass and “Rest-visible Color”, and the LRDs do not show a significant bias in black hole mass given their host galaxy mass. As discussed above, overmassive black holes play a crucial role in the appearance of sources as LRDs, so this lack of correlation between black hole mass and redness, is likely due to two factors. First, all of the black holes in this BRAHMA simulation are significantly overmassive relative to ASTRID galaxies of similar stellar mass, so even the lower mass black holes in BRAHMA are sufficiently massive enough to produce AGN spectra that can power an LRD. Second, there may be a weaker relationship between red color and black hole mass in the mass range of BRAHMA but the simulation volume is not sufficient to make that relationship clear.

In figure 5 we show the bolometric luminosity of the black holes present in each galaxy in relation to their masses, and the stellar mass of their host galaxies. The BRAHMA black holes are dimmer at a given mass compared to ASTRID, and are accreting significantly below the Eddington limit. This sub-Eddington accretion is at odds with the original application of the “gas-enshrouded” AGN model to LRDs, which was associated with super-Eddington accretion in Inayoshi & Maiolino (2025). That said, other works which use similar models, conclude it may also be applicable in a scenario with “heavy seeds” (Naidu et al. 2025; Taylor et al. 2025) potentially as a result of direct collapse black holes (DCBHs) (Jeon et al. 2025). One of the proposed fits from Naidu et al. (2025) of the  $z \approx 7.7$  LRD they analyzed, featured minimal dust, significant gas absorption, and selected a black hole of mass  $\log(M_{\text{BH}} / M_{\odot}) = 7.7$  and a bolometric luminosity of  $\log(L_{\text{bol}} / \text{ergs}^{-1}) = 45.0$  (Edd. ratio of 0.16), which would lie just above the LRDs found in BRAHMA.

The brightness of black holes in galaxies of a given mass is relatively consistent between BRAHMA and ASTRID due to the shift in the  $M_{\text{BH}} - M_*$  relation shown in figure 4. There is a strong correlation between higher bolometric luminosity and “Rest-visible Color”, with sources hosting brighter black holes being significantly redder, and all of the LRDs in BRAHMA containing black holes with a bolometric luminosity of  $\log(L_{\text{bol}} / \text{ergs}^{-1}) \geq 42.9$ . This is expected as the large Balmer break present in the “gas-enshrouded” AGN SED model will have a significant impact on the color for sources whose AGN contributes a larger portion of the visible light.

Notably, there is significant overlap between the region of  $L_{\text{bol}} - M_*$  space where the LRDs found in BRAHMA lie, and the general ASTRID population, and there are some LRDs found in ASTRID there. While the total number of LRDs in this region appears comparable between the two

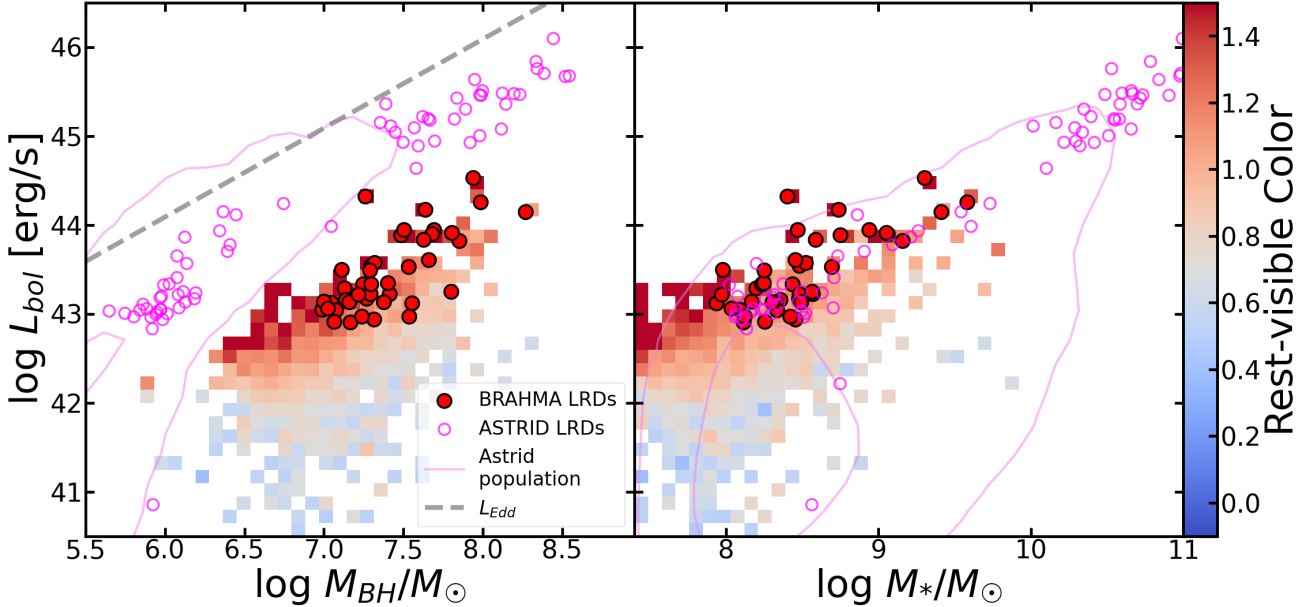


FIG. 5.—  $L_{\text{bol}} - M_{\text{BH}}$  and  $L_{\text{bol}} - M_{*}$  for the black holes and their host galaxies in the **BRAHMA** and **ASTRID** simulations. The 2D histogram shows the overall **BRAHMA** population. It is colored by the mean “Rest-visible Color” in each cell, where “Rest-visible Color” is  $F200W-F356W$  for  $z=5,6$  sources, and  $F277W-F444W$  for  $z=7,8$  sources. The magenta contours contain  $1\sigma$  and  $3\sigma$  of sources in the **ASTRID** simulation. The dashed grey line in the left panel indicates the Eddington luminosity as a function of black hole mass.

simulations, **ASTRID** has  $1000\times$  more simulation volume than the **BRAHMA** simulation we analyzed, so the number density of LRDs in this region is  $\sim 1000\times$  higher in **BRAHMA** than **ASTRID**. This reinforces the importance of the overmassive black holes present in this **BRAHMA** simulation.

We compare the bolometric luminosity function of the LRDs in **BRAHMA** in the two redshift ranges ( $z = 5 \sim 6$  and  $z = 7 \sim 8$ ) to those from observations of LRDs in similar redshift ranges in figure 6. Comparing to the observations using conventional bolometric corrections (Kokorev et al. 2024; Greene et al. 2024) **BRAHMA** contains more LRDs with black holes that are less luminous. Recently Greene et al. (2025) suggested an alternative bolometric correction for AGN in this epoch, which shifts their pre-correction bolometric luminosity function (purple squares) roughly one dex to the left (post-correction points shown as blue squares), producing a luminosity function that is mostly consistent with our results.

In both cases, there is a relative overabundance of dimmer AGN in LRDs in this **BRAHMA** simulation. This could be due to the lenient black hole seeding and dynamics models used in **BRAHMA**. Alternatively, it could also be a result of the “gas-enshrouded” AGN model being applied to all AGN in the simulation. It is possible that the proportion of AGN that are shrouded in a cloud of dense gas is below 100%, which would lower the number density of LRDs.

At the brighter end of the distribution, this **BRAHMA** simulation under-predicts the number of LRDs containing a black hole with  $L_{\text{bol}} \geq 10^{45}$  relative to most observations. This may be due to the limited simulation volume of **BRAHMA**, which we intend to investigate with higher volume simulations in future work. If this under-prediction is still present in a larger volume, that suggests either the adjustments to bolometric corrections made in Greene et al. (2025) are correct (as the LF of this **BRAHMA** realization is consistent with that dataset) or the lenient

black hole seeding and dynamics models are suppressing the number of LRD that contain  $L_{\text{bol}} \geq 10^{45}$  AGN. In the latter case, further analysis would be necessary to determine if adjustments could be made to the black hole models of this **BRAHMA** simulation that maintain its agreement with observations in other areas, while reproducing the bright AGN seen in observations. Such changes may also result in some black holes with accretion rates closer to the Eddington limit, which would be more consistent with early “gas-enshrouded AGN” works like Inayoshi & Maiolino (2025).

### 3.3. What Makes an LRD

The LRDs in **BRAHMA** have host galaxies with stellar masses  $10^{8.0} M_{\odot} \leq M_{*} \leq 10^{9.75} M_{\odot}$ , and black holes with bolometric luminosities  $\log(L_{\text{bol}}/\text{ergs}^{-1}) \geq 42.9$ . This alone is not sufficient for an object to appear as an LRD, as **ASTRID** also contains many sources with those properties, but very few appear as LRDs as discussed above.

The differentiating property of the **BRAHMA** sources is their significantly higher black hole mass relative to their **ASTRID** counterparts. For a given luminosity, the higher mass black holes in **BRAHMA** will have low temperature AGN spectra than the lower mass black holes in **ASTRID**. The SED of a lower temperature AGN peaks at a longer wavelength, resulting in a spectrum that is brighter in the rest-optical compared to a higher temperature AGN with the same luminosity. This can be seen in figure 1. The dashed grey line is the incident SED for an AGN with a temperature of  $T = 10^{4.5}\text{K}$ . It is twice as bright in the F444W filter than the  $T = 10^{5.5}\text{K}$  SED with the same luminosity (the dotted grey line). This makes the emission of the higher mass AGN more prominent in the long wavelength JWST bands relative to its host galaxy, and emphasizes its Balmer break, when compared to its lower mass counterpart. This results in the higher mass black holes in **BRAHMA** producing spectra that are brighter

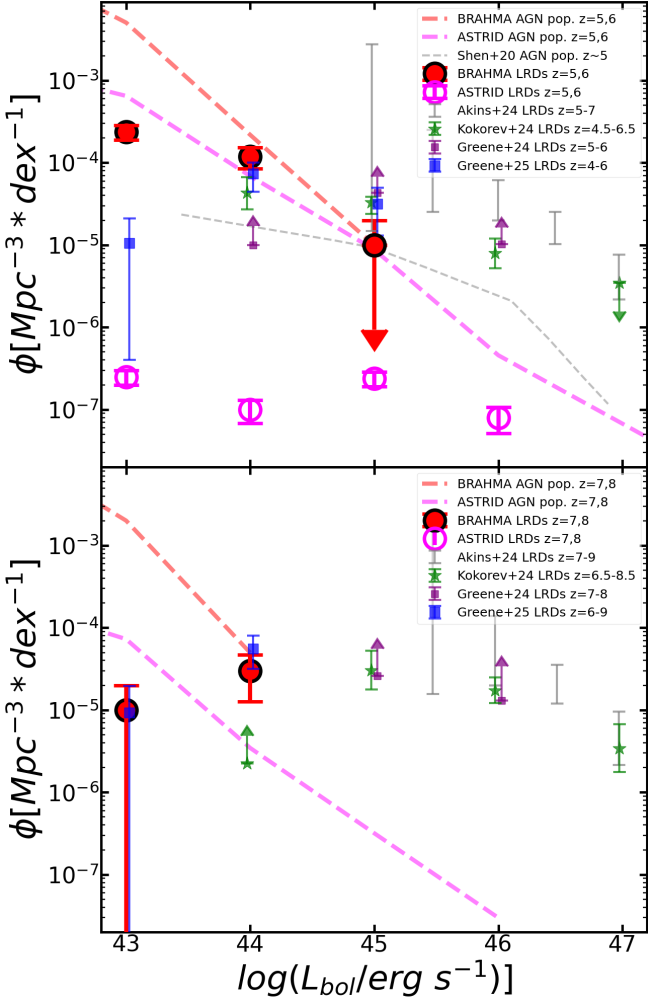


FIG. 6.— The bolometric luminosity function of the AGN for datasets around  $5 \leq z \leq 6$  (top panel), and  $7 \leq z \leq 8$  (bottom panel). The AGN found in LRDs in **BRAHMA** are shown with red circles, and the **ASTRID** LRDs are shown with magenta circles (Not seen on the bottom panel due to falling below the x-axis). We compare with the luminosity functions of multiple observations (Kokorev et al. 2024; Akins et al. 2025) including both pre and post correction sets from Greene et al. (2025). We also include the overall AGN luminosity function of **BRAHMA**, **ASTRID**, and **Shen** et al. (2020) as dashed lines.

and redder in the rest-optical than the lower mass black holes with the same luminosity in **ASTRID**. As these two quantities are vital to a source being detectable, and classified as an LRD, the higher mass **BRAHMA** black holes are far more likely to be identified as LRDs.

In Figure 7, we analyze the contribution of the AGN and the host galaxy, and the amount of dust attenuation in both the F444W and F150W bands. The LRDs in both **BRAHMA** and **ASTRID** have significant AGN contributions to their observed F444W emission, but their shorter wavelength F150W emission is generally dominated by the host galaxy. This indicates a hybrid AGN+galaxy model is likely necessary to accurately reproduce all of the spectral features present in LRDs.

In the lower panels of figure 7 we see that the **BRAHMA** LRD population generally shows very minimal attenuation, especially in the longer wavelengths, with mean and standard deviation of the attenuation in the F444W  $A_{F444W} = 0.15 \pm 0.09$ . We also compute the rest frame

visible attenuation based on the NIRCam filter centered nearest to the V-band (F356W for  $z=5,6$  and F444W for  $z=7,8$ ), and find  $A_V = 0.21 \pm 0.12$ . While we do not model dust re-emission in the current pipeline, it is extremely unlikely that the minimal amount of attenuated light in the **BRAHMA** LRDs would be sufficient to produce enough re-emission in the infrared to exceed the current observational limits. As a lower bound on the emission in this region we calculate the luminosity of one of the brightest AGN among the LRDs ( $\log(M_{BH}/M_\odot) = 7.94$ ,  $\log(L_{bol}/\text{ergs}^{-1}) = 44.5$ ,  $z=6$ ) in the ALMA 1.2mm band to be  $\nu L_\nu = 5.9 * 10^6 L_\odot$ , which is less than 1% of the ALMA upper limits ( $\nu L_\nu \sim 10^9 L_\odot$ ) (Casey et al. 2025; Setton et al. 2025; Xiao et al. 2025; Akins et al. 2025).

Given the high AGN contribution to LRD emission in **BRAHMA** and the substantial variation in black hole accretion rates on very short timescales, we investigate the recent history of black hole accretion in the LRDs. We average the accretion rate of each black hole over the last 25 Myr in order to capture the short term variability of the black hole's accretion, while limiting the impact of longer term trends in the black hole's accretion. We find that most of the black holes are accreting at a rate that is similar to their mean accretion rate from the previous 25 Myr ( $M_{obs} = 1.11_{-0.77}^{+1.00} [M_{\text{mean,25Myr}}]$ ). This indicates the LRDs identified in **BRAHMA** do not rely on brief spikes in accretion to appear as LRDs. We intend to perform a more in-depth analysis of the accretion rate histories of AGN in LRDs in future work, which could determine the duty cycle and expected lifetime of LRDs,

#### 4. DISCUSSION AND MODELING CAVEATS

Our work is a follow-up to our previous exploration of LRDs in the **ASTRID** simulation LaChance et al. (2025) in two distinct ways. First, as **ASTRID** does not contain the overmassive BH population indicated by current JWST measurements, we use a **BRAHMA** realization that produced such overmassive BHs via a lenient seeding model. Second, we use an updated AGN SED model assuming a “gas-enshrouded” AGN as proposed in multiple recent papers (Inayoshi & Maiolino 2025; Naidu et al. 2025; Taylor et al. 2025; Jeon et al. 2025).

The abundant formation and frequent mergers of heavy  $\sim 10^5 M_\odot$  seeds in the black hole seeding model enable the production of an overmassive black hole population in the **BRAHMA** simulations at high redshift, making them an excellent testbed for exploring the implications of overmassive black holes for LRDs. However, it remains unclear whether such efficient heavy-seed production is feasible in nature, as traditional direct-collapse formation scenarios are thought to be highly restrictive due to their requirement of strong Lyman-Werner radiation fields. That said, several alternative mechanisms have been proposed that could yield heavy seeds in larger numbers without requiring such extreme Lyman-Werner fluxes. These include rapid stellar or black hole mergers in dense star clusters (Davies et al. 2011; Dekel et al. 2025), as well as early episodes of rapid or hyper-Eddington accretion onto lower-mass seeds embedded in dense gas clumps (Mehta et al. 2024; Prole et al. 2025). In addition, while Bhowmick et al. (2024c) found that merger delay times of  $\lesssim 750$  Myr are required to assemble overmassive black holes through mergers, the true merger timescales remain highly uncertain, particularly when ac-

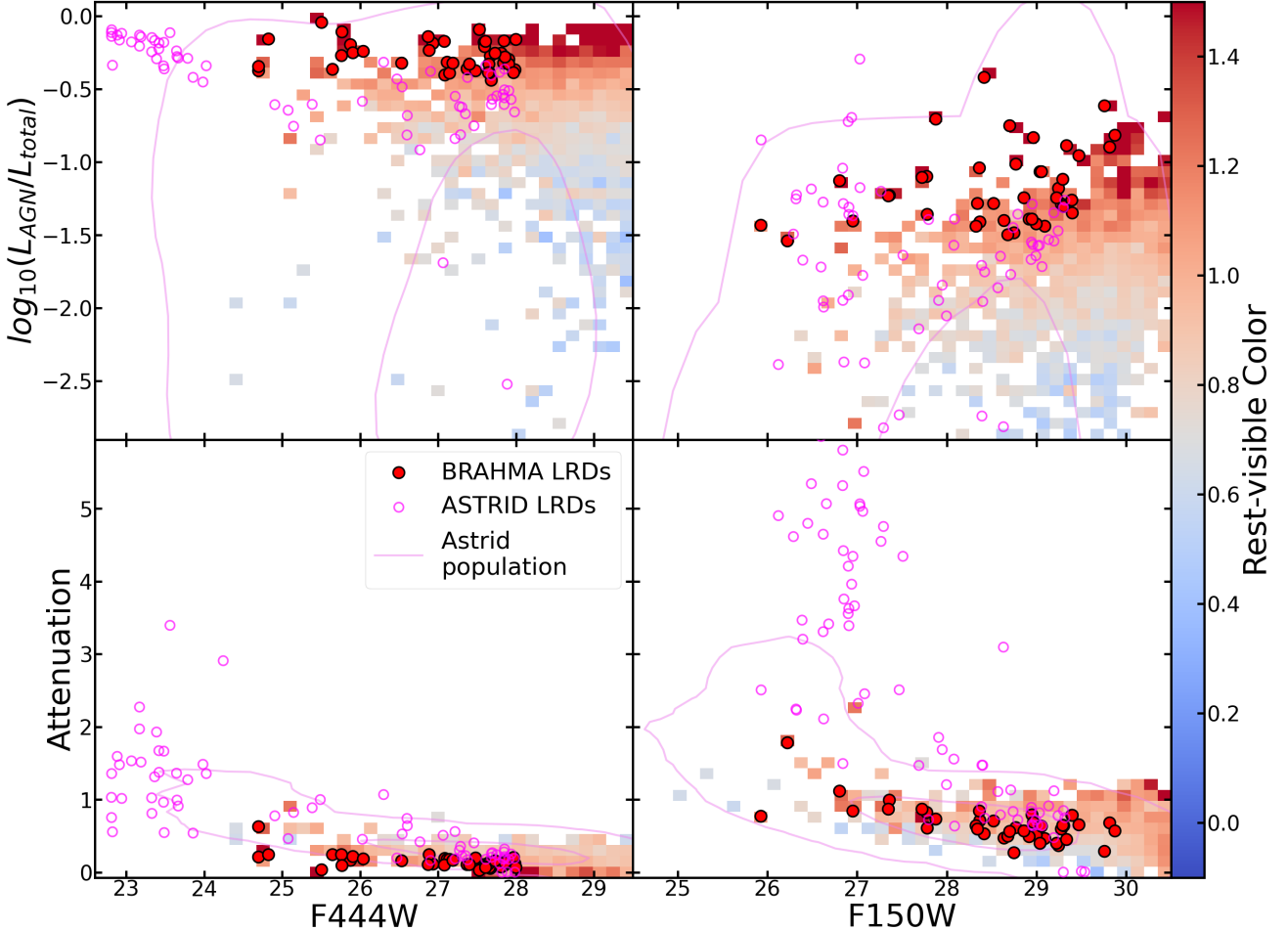


FIG. 7.— The top row shows the relative contribution of the AGN to the overall emission in both the F444W and F150W bands. The bottom row shows the amount of dust attenuation experienced by each source in the F444W and F150W bands. The x-axis of each plot is the source magnitude in the relevant filter (F444W for the left column, F150W for the right column). The 2D histogram shows the overall BRAHMA population. It is colored by the mean “Rest-visible Color” in each cell, where “Rest-visible Color” is F200W-F356W for  $z=5,6$  sources, and F277W-F444W for  $z=7,8$  sources. The magenta contours contain  $1\sigma$  and  $3\sigma$  of sources in the ASTRID simulation.

counting for effects such as gravitational recoil. Alternatively, if merger-driven growth turns out to be not efficient enough, producing overmassive black holes at high redshift may require reduced AGN feedback efficiencies (relative to standard assumptions), allowing sustained growth through gas accretion (Bhowmick et al. 2025; Bhowmick et al., in prep). Overall, while the detailed pathways leading to the assembly of overmassive black holes at high redshift are not yet fully constrained, our results demonstrate that their overmassiveness—combined with heavy enshrouding by dense gas—is a critical ingredient for producing AGN-dominated LRDs.

The overmassiveness of the black holes in this BRAHMA simulation, and the sub-Eddington accretion they exhibit, aligns most closely with the “heavy seeds experiencing Eddington-limited accretion” formation pathway for LRDs. Recent works such as Taylor et al. (2025) and Jeon et al. (2025) suggest this formation pathway is compatible with the “gas-enshrouded” AGN model. Similar to our findings, their results indicate this formation pathway, and AGN emission model can produce an LRD population that is comparable to observations. This is in contrast to the works which established this AGN emission model including Naidu et al. (2025), and

Inayoshi & Maiolino (2025), which aligned more closely with the “light seeds undergoing super-Eddington accretion” formation pathway. These works also indicated the masses of AGN in the early universe may be overestimated, which is not compatible with the black hole population of this BRAHMA simulation. Our findings suggest that higher mass black holes are favored over lower mass black holes for LRD production due to their lower temperature at a given accretion rate, which causes more of their emission to be produced in the rest-visible wavelengths. That said, if the black holes in the “light seeds” scenario are able to accrete at a higher rate than their “heavy seed” counterparts in similar host halos, the increase in bolometric luminosity from the elevated accretion could compensate for their AGN SED being intrinsically dimmer in the rest-visible range.

Even under the “heavy seeds experiencing Eddington-limited accretion” LRD formation umbrella, the significantly sub-Eddington accretion seen in the AGN population of BRAHMA is an outlier. When considered alongside the deficit of LRDs with AGN with  $\log(L_{bol}/\text{ergs}^{-1}) \geq 45.0$  relative to some observational data sets, this suggests that adjustments could be made to the models employed in this simulation that would produce a popu-

lation of LRDs that is in closer alignment with observations. We intend to explore this possibility in future work.

Additionally, for probing rare objects such as LRDs, the simulation volume of **BRAHMA** limits some possible avenues of analysis. For this reason, we intend to perform a similar analysis on a larger-volume simulation that uses a similar black hole seeding model. This should enable a variety of new analyses, including investigating: (i) the evolution of the LRD population over time, (ii) the percentage of galaxies which could host “gas-enshrouded” AGN, (iii) what black hole and/or galaxy properties are correlated with these environments, and (iv) identifying counterparts to the rarer brighter objects that have been observed. Specifically, we intend to produce a realization of the **ASTRID** simulation with the **BRAHMA** black hole seeding model, which will offer a significantly larger volume, and isolate the impact of the black hole seeding model, as it will be identical to **ASTRID** in all other aspects including the treatment of subgrid dynamical friction and mergers.

Finally, a further development of the mock observation pipeline would provide unique insights into the nature of these objects. Specifically, implementing and analyzing a grid of AGN emission models in **CLOUDY** to determine if there are any thresholds in parameters like the volume density and surface density of hydrogen, which drastically affect the number of LRDs. A systematic search of the AGN SED parameters to identify which combination(s) produce a population of LRDs that matches most accurately with observations would provide some clarity on the shape of the SED of AGN in these objects. We also plan to implement dust re-emission which would enable a range of analyses of LRD dust properties, augmenting observational dust constraints. We intend to add this functionality to our mock observation pipeline via the mock observation software **SYNTESIZER** (Lovell et al. 2025).

## 5. CONCLUSIONS

In this work, we produce mock observations of AGN and their host galaxies in one of the volumes from the **BRAHMA** simulation suite that yields the most strongly overmassive black holes, in order to investigate their potential role in the formation of “little red dots” (LRDs). In light of the recent emphasis on the Balmer break in LRDs (Setton et al. 2024; Inayoshi & Maiolino 2025; Liu et al. 2025), and the advent of new AGN emission models involving dense gas clouds, we employ a gas-enshrouded AGN emission model for these sources. We use this model to analyze AGN in **BRAHMA** snapshots at  $z = 5, 6, 7$ , and  $8$ , spanning the redshift range that encompasses the bulk of JWST LRD detections. We apply the observed selection criteria to identify LRDs in these snapshots and compare our results against the **ASTRID** simulation, which produces systematically smaller black holes at fixed galaxy mass at these redshifts. We draw the following conclusions:

1. We identify 41 LRDs across all four **BRAHMA** snapshots, with an average number density of  $2.0 \times 10^{-4} \text{Mpc}^{-3}$ . This represents an upper bound on the LRD density (see, e.g., Pacucci & Loeb 2025) in

this simulation with these models, as it is unlikely that all AGN in this epoch are “gas-enshrouded”.

2. By number density this LRD population is in much closer agreement with current observations than the LRD population produced in the **ASTRID** simulations, which underpredicts the number density of LRDs by more than two orders of magnitude when processed with both the standard and “gas-enshrouded” AGN models.
3. When this **BRAHMA** realization is analyzed using a standard AGN SED, it also produces significantly fewer LRDs than inferred from observations ( $\sim 1$  order of magnitude), suggesting that both overmassive black holes and AGN residing in very dense gaseous environments play a key role in reproducing the observed LRD population.
4. The LRD host galaxies in the **BRAHMA** simulation have stellar masses in the range  $10^8 \leq M_*/M_\odot \leq 10^{9.75}$ , and black hole masses exceeding  $\sim 10^7 M_\odot$  that are accreting below the Eddington limit, producing bolometric luminosities  $42.9 \leq \log(L_{\text{bol}}/\text{ergs}^{-1}) \leq 44.5$ .
5. In the LRDs present in **BRAHMA** the AGN contribute significantly to the emission of all the LRDs in the rest-frame visible above the Balmer break, and are responsible for the significant red color that is emblematic of LRDs. As such, sources with black holes that are bright relative to their host galaxies are far more likely to appear as LRDs.
6. The LRD sources in **BRAHMA** experience minimal attenuation ( $A_V = 0.19^{+0.09}_{-0.06}$ ), which limits the potential for infrared re-emission, aligning with the observed infrared limits from ALMA.

These findings lead us to conclude that a population of overmassive black holes that are enveloped in a cloud of dense gas is required for an AGN-centric LRD model to reproduce the number density of LRDs observed with JWST.

## ACKNOWLEDGMENTS

AKB and PT acknowledge support from NSF-AST 2510738, NSF-AST 2346977, and the NSF-Simons AI Institute for Cosmic Origins which is supported by the National Science Foundation under Cooperative Agreement 2421782 and the Simons Foundation award MPS-AI-00010515. TDM acknowledges funding from NASA ATP 80NSSC20K0519, NSF PHY-2020295, NASA ATP NNX17AK56G, and NASA ATP 80NSSC18K101, NASA Theory grant 80NSSC22K072. TDM and YZ acknowledge the support from the NASA FINESST grant NNH24ZDA001N. FP acknowledges support by the Black Hole Initiative at Harvard University. LB acknowledges support from NSF award AST-2307171 and NASA award 80NSSC22K0808. YN acknowledges support from the ITC Postdoctoral Fellowship. NC acknowledges support from the Schmidt Futures Fund. SB acknowledges funding from NASA ATP 80NSSC22K1897 and NSF AST-2509639. **ASTRID** was run on the Frontera facility at the Texas Advanced Computing Center.

## REFERENCES

Akins H. B., et al., 2025, *ApJ*, **991**, 37

Ananna T. T., Bogdán Á., Kovács O. E., Natarajan P., Hickox R. C., 2024, *ApJ*, **969**, L18

Baggen J. F. W., et al., 2023, *ApJ*, **955**, L12

Baggen J. F. W., et al., 2024, *ApJ*, **977**, L13

Barnes J., Hut P., 1986, *Nature*, **324**, 446

Barro G., et al., 2023, *arXiv e-prints*, p. arXiv:2305.14418

Bhowmick A. K., et al., 2021, *MNRAS*, **507**, 2012

Bhowmick A. K., Blecha L., Torrey P., Kelley L. Z., Vogelsberger M., Nelson D., Weinberger R., Hernquist L., 2022, *MNRAS*, **510**, 177

Bhowmick A. K., Blecha L., Torrey P., Weinberger R., Kelley L. Z., Vogelsberger M., Hernquist L., Somerville R. S., 2024a, *MNRAS*, **529**, 3768

Bhowmick A. K., et al., 2024b, *MNRAS*, **531**, 4311

Bhowmick A. K., et al., 2024c, *MNRAS*, **533**, 1907

Bhowmick A. K., et al., 2025, *arXiv e-prints*, p. arXiv:2510.01322

Bird S., Ni Y., Di Matteo T., Croft R., Feng Y., Chen N., 2022, *MNRAS*, **512**, 3703

Brooks M., et al., 2024, *arXiv e-prints*, p. arXiv:2410.07340

Brooks M., et al., 2025, *arXiv e-prints*, p. arXiv:2511.19609

Calzetti D., Armus L., Bohlin R. C., Kinney A. L., Koornneef J., Storchi-Bergmann T., 2000, *ApJ*, **533**, 682

Casey C. M., Akins H. B., Kokorev V., McKinney J., Cooper O. R., Long A. S., Franco M., Manning S. M., 2024, *ApJ*, **975**, L4

Casey C. M., et al., 2025, *ApJ*, **990**, L61

Chen N., Ni Y., Tremmel M., Di Matteo T., Bird S., DeGraf C., Feng Y., 2022, *MNRAS*, **510**, 531

Davies M. B., Miller M. C., Bellvary J. M., 2011, *ApJ*, **740**, L42

Dekel A., Stone N. C., Chowdhury D. D., Gilbaum S., Li Z., Mandelker N., van den Bosch F. C., 2025, *A&A*, **695**, A97

Durodola E., Pacucci F., Hickox R. C., 2025, *ApJ*, **985**, 169

Feng Y., Di-Matteo T., Croft R. A., Bird S., Battaglia N., Wilkins S., 2016, *MNRAS*, **455**, 2778

Feng Y., Bird S., Anderson L., Font-Ribera A., Pedersen C., 2018, Mp-Gadget/Mp-Gadget: A Tag For Getting A Doi, Zenodo, doi:10.5281/zenodo.1451799

Furtak L. J., et al., 2023, *ApJ*, **952**, 142

Furtak L. J., et al., 2024, *Nature*, **628**, 57

Greene J. E., et al., 2024, *ApJ*, **964**, 39

Greene J. E., et al., 2025, *arXiv e-prints*, p. arXiv:2509.05434

Guia C. A., Pacucci F., Kocevski D. D., 2024, *Research Notes of the American Astronomical Society*, **8**, 207

Gunasekera C. M., et al., 2025, *arXiv e-prints*, p. arXiv:2508.01102

Hahn O., Abel T., 2011, *MNRAS*, **415**, 2101

Harikane Y., et al., 2023, *ApJ*, **959**, 39

Hviding R. E., et al., 2025, *A&A*, **702**, A57

Inayoshi K., Maiolino R., 2025, *ApJ*, **980**, L27

Jeon J., et al., 2025, *arXiv e-prints*, p. arXiv:2508.14155

Jones B. L., et al., 2025, *arXiv e-prints*, p. arXiv:2510.07376

Juodžbalis I., et al., 2025, *arXiv e-prints*, p. arXiv:2504.03551

Katz N., Weinberg D. H., Hernquist L., 1996, *ApJS*, **105**, 19

Kocevski D. D., et al., 2023, *ApJ*, **954**, L4

Kocevski D. D., et al., 2025, *ApJ*, **986**, 126

Kokorev V., et al., 2024, *ApJ*, **968**, 38

Krumholz M. R., Gnedin N. Y., 2011, *ApJ*, **729**, 36

LaChance P., Croft R., Ni Y., Chen N., Di Matteo T., Bird S., 2024, *arXiv e-prints*, p. arXiv:2401.16608

LaChance P., Croft R. A. C., Di Matteo T., Zhou Y., Pacucci F., Ni Y., Chen N., Bird S., 2025, *arXiv e-prints*, p. arXiv:2505.20439

Labbé I., et al., 2023, *Nature*, **616**, 266

Labbé I., et al., 2024, *arXiv e-prints*, p. arXiv:2412.04557

Labbé I., et al., 2025, *ApJ*, **978**, 92

Liu H., Jiang Y.-F., Quataert E., Greene J. E., Ma Y., 2025, *ApJ*, **994**, 113

Lovell C. C., Roper W. J., Vijayan A. P., Wilkins S. M., Newman S., Seeyave L., 2025, *The Open Journal of Astrophysics*, **8**, 152

Ma L., Hopkins P. F., Ma X., Anglés-Alcázar D., Faucher-Giguère C.-A., Kelley L. Z., 2021, *MNRAS*, **508**, 1973

Ma Y., et al., 2024, *arXiv e-prints*, p. arXiv:2410.06257

Maiolino R., et al., 2024, *A&A*, **691**, A145

Maiolino R., et al., 2025, *MNRAS*, **538**, 1921

Marinacci F., et al., 2018, *MNRAS*, **480**, 5113

Matthee J., et al., 2023, *arXiv e-prints*, p. arXiv:2306.05448

Mehta D., Regan J. A., Prole L., 2024, *The Open Journal of Astrophysics*, **7**, 107

Naidu R. P., et al., 2025, *arXiv e-prints*, p. arXiv:2503.16596

Naiman J. P., et al., 2018, *MNRAS*, **477**, 1206

Nelson D., et al., 2018, *MNRAS*, **475**, 624

Nelson D., et al., 2019, *Computational Astrophysics and Cosmology*, **6**, 2

Ni Y., et al., 2022, *MNRAS*, **513**, 670

Ni Y., Chen N., Zhou Y., Park M., Yang Y., Di Matteo T., Bird S., Croft R., 2025, *ApJ*, **990**, 120

Pacucci F., Loeb A., 2024, *ApJ*, **964**, 154

Pacucci F., Loeb A., 2025, *ApJ*, **989**, L19

Pacucci F., Narayan R., 2024, *ApJ*, **976**, 96

Pacucci F., Nguyen B., Carniani S., Maiolino R., Fan X., 2023, *ApJ*, **957**, L3

Pacucci F., Hernquist L., Fujii M., 2025, *ApJ*, **994**, 40

Pakmor R., Bauer A., Springel V., 2011, *MNRAS*, **418**, 1392

Pakmor R., Pfrommer C., Simpson C. M., Kannan R., Springel V., 2016, *MNRAS*, **462**, 2603

Partmann C., Naab T., Rantala A., Genina A., Mannerkoski M., Johansson P. H., 2024, *MNRAS*, **532**, 4681

Pei Y. C., 1992, *ApJ*, **395**, 130

Pérez-González P. G., et al., 2024, *ApJ*, **968**, 4

Perger K., Fogasy J., Frey S., Gabányi K. É., 2025, *A&A*, **693**, L2

Pillepich A., et al., 2018, *MNRAS*, **475**, 648

Planck Collaboration et al., 2016, *A&A*, **594**, A13

Planck Collaboration et al., 2020, *A&A*, **641**, A6

Prole L. R., et al., 2025, *arXiv e-prints*, p. arXiv:2511.09640

Rahmati A., Pawlik A. H., Raičević M., Schaye J., 2013, *MNRAS*, **430**, 2427

Reines A. E., Völneri M., 2015, *ApJ*, **813**, 82

Schaye J., et al., 2015, *MNRAS*, **446**, 521

Setton D. J., et al., 2024, *arXiv e-prints*, p. arXiv:2411.03424

Setton D. J., et al., 2025, *arXiv e-prints*, p. arXiv:2503.02059

Shen X., Hopkins P. F., Faucher-Giguère C.-A., Alexander D. M., Richards G. T., Ross N. P., Hickox R. C., 2020, *MNRAS*, **495**, 3252

Springel V., 2010, *MNRAS*, **401**, 791

Springel V., Hernquist L., 2003, *MNRAS*, **339**, 289

Springel V., et al., 2018, *MNRAS*, **475**, 676

Stanway E. R., Eldridge J. J., 2018, *MNRAS*, **479**, 75

Stone M. A., Lyu J., Rieke G. H., Alberts S., Hainline K. N., 2024, *ApJ*, **964**, 90

Taylor A. J., et al., 2024, *arXiv e-prints*, p. arXiv:2409.06772

Taylor A. J., et al., 2025, *ApJ*, **989**, L7

Übler H., et al., 2023, *A&A*, **677**, A145

Vijayan A. P., Lovell C. C., Wilkins S. M., Thomas P. A., Barnes D. J., Irodotou D., Kuusisto J., Roper W. J., 2021, *MNRAS*, **501**, 3289

Wang B., et al., 2024, *ApJ*, **969**, L13

Weinberger R., Springel V., Pakmor R., 2020, *ApJS*, **248**, 32

Wilkins S. M., Feng Y., Di Matteo T., Croft R., Lovell C. C., Waters D., 2017, *MNRAS*, **469**, 2517

Wilkins S. M., et al., 2020, *Monthly Notices of the Royal Astronomical Society*, **493**, 6079

Xiao M., et al., 2025, *arXiv e-prints*, p. arXiv:2503.01945

Yue M., et al., 2024a, *ApJ*, **966**, 176

Yue M., Eilers A.-C., Ananna T. T., Panagiotou C., Kara E., Miyaji T., 2024b, *ApJ*, **974**, L26

Zhou Y., et al., 2025, *arXiv e-prints*, p. arXiv:2510.13976

de Graaff A., et al., 2025, *arXiv e-prints*, p. arXiv:2503.16600

provides fast and easy peer review for new papers in the `astro-ph` section of the arXiv, making the reviewing process simpler for authors and referees alike. Learn more at <http://astro.theoj.org>.